

Supporting Information for

Layer Number dependent Optoelectronic Characteristics of quasi-2D

PBA₂(MAPbBr₃)_{n-1}PbBr₄ perovskite films

Lianfei Yao^a, Xue Lou^a, Ning Sui*^a, Zhihui Kang^a, Qiang Zhou^b, Li Li^c, Bing Zhao^d, Han-zhuang Zhang^a, Jiaqi Zhang*^e, Yinghui Wang*^a.

^a Femtosecond Laser laboratory, Key Laboratory of Physics and Technology for Advanced Batteries (Ministry of Education), College of Physics, Jilin University, Changchun 130012, China.

^b State Key Laboratory of Superhard Materials, College of Physics, Jilin University, Changchun 130012, China.

^c College of Physics and Optoelectronic Engineering, Harbin Engineering University, Harbin, 150001, China.

^d State Key Laboratory of Supramolecular Structure and Materials, Jilin University, Changchun 130012, China.

^e Key Laboratory of Automobile Materials, Ministry of Education, College of Materials Science and Engineering, Jilin University, Changchun 130012, China.

S1. Fit to FWHM of PL Spectra under Different Temperature

The integrated PL intensity (IPLI) and FWHM of the PL spectra are calculated through full peak fitting to PL spectrum. The emission line width dependent on temperature can be described by a Bose-Einstein statistics:

$$\Gamma(T) = \Gamma_0 + \Gamma_{LA}T + \Gamma_{LO} \frac{1}{e^{\frac{E_{LO}/k_B T}{}} - 1} + \gamma_{imp} \frac{1}{e^{-\frac{E_b/k_B T}{}}}$$

Here, Γ_0 is inhomogeneous broadening term independent on temperature. Γ_{LA} is homogeneous broadening term, arising from acoustic phonon scattering. Γ_{LO} and E_{LO} are scattering intensity and energy of longitudinal optical (LO) phonon, respectively. And the last term denotes the contribution of impurities on the line width, which is neglected in further calculation.

The broadening of FWHM with the temperature is much dependent of the carrier scattering caused by carrier-phonon interaction. In general, there are four sources to scatter the carriers causing broadening the PL, inhomogeneous broadening without temperature dependence, acoustic phonon scattering, LO phonon scattering via the Fröhlich interaction and impurities scattering, respectively. However, if impurity contribution is dominant at PL broadening, there will be a saturation at high temperature in the temperature dependence of FWHM. Or, in the case of dominant scattering by acoustic phonons, the line width broadens linearly with increasing temperature.

S2. Fit to the PL Intensity under Different Temperatures

The trend of PL intensity with temperature can be expressed by the Arrhenius equation:

$$I(T) = I_0 / (1 + Ae^{-E_B/k_B T})$$

where I_0 is the intensity at 0 K; k_B is Boltzmann constant and E_B is exciton binding energy.

S3. Calculation of Temperature-Dependent PLQY

The PL quantum yield (QY) can be defined as the ratio of the number of emitted photons to the number of absorbed photons by a luminescent material:

$$QY = \frac{N_{em}}{N_{abs}} = \frac{\int \frac{\lambda}{hc} [I_{em}^{sample}(\lambda) - I_{em}(\lambda)] d\lambda}{\int \frac{\lambda}{hc} [I_{ex}(\lambda) - I_{ex}^{sample}(\lambda)] d\lambda}$$

The most straightforward method for the determination of QY values presents the absolute measurement of N_{abs} and N_{em} with an integrating sphere setup. Here, λ is the wavelength; h is Planck's constant; c is the velocity of light; I_{ex}^{sample} and I_{ex} are the integrated intensities of the excitation light with and without a sample, respectively.

The PLQY at low temperature QY_2 can be obtained from QY_1 at room temperature:

$$\frac{QY_2}{QY_1} = \frac{I_{em2}}{I_{em1}} \times \frac{A_1}{A_2} \times \frac{\lambda_{ex1}}{\lambda_{ex2}} \times \frac{\eta_2}{\eta_1}$$

Here, I_{em} is the integrated area under the corrected emission spectrum; A is the absorbance at the excitation wavelength; λ_{ex} is the excitation wavelength; η is the collection efficiency of the system.

S4. Derivation of radiative lifetimes from measured PL dynamics

The PL decay can be described by:

$$I_{PL}(t) = \sum_{i=1}^n k_i \exp(-t/\tau_X^i)$$

where τ_X^i is the effective lifetime given by:

$$\tau_X^i = \tau_{r,X} \tau_{nr,X}^i / (\tau_{r,X} + \tau_{nr,X}^i)$$

k_i is the relative fraction of perovskite film in the i -th sub-ensemble.

The PLQY of the individual sub-ensemble is given by:

$$q_i = \tau_X^i / \tau_{r,X}$$

And the total PLQY of the entire sample (Q) can be expressed as:

$$Q = \sum_{i=1}^n k_i q_i = \tau_{r,X}^{-1} \sum_{i=1}^n k_i \tau_X^i$$

So, the radiative lifetime is expressed as:

$$\tau_{r,X} = Q^{-1} \sum_{i=1}^n k_i \tau_X^i = Q^{-1} \langle \tau_X \rangle$$

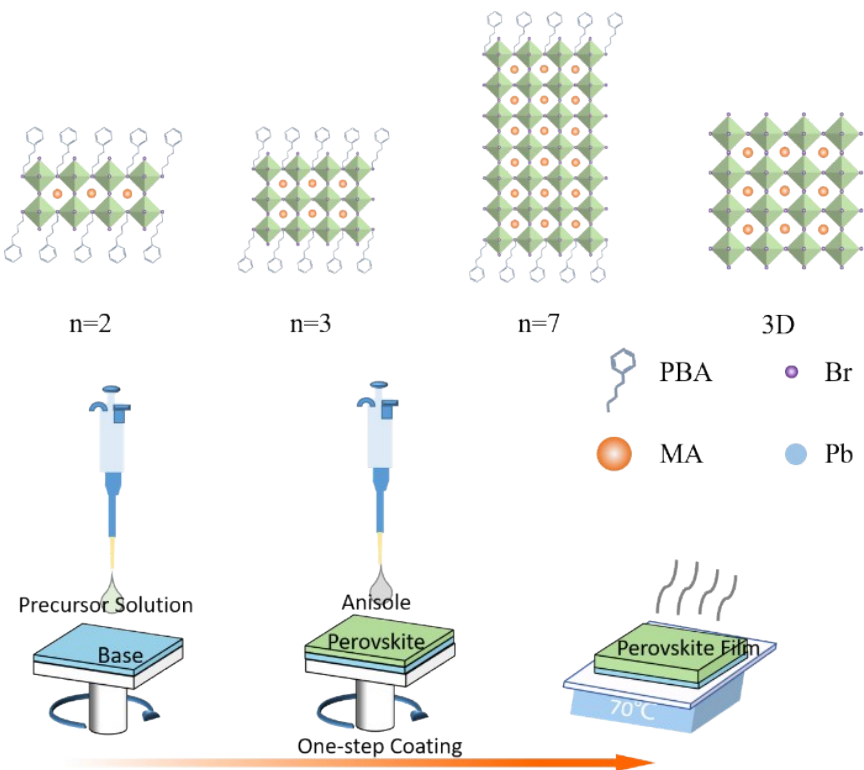
where $\langle \tau_X \rangle$ is the average lifetime.

S5. The exciton binding energy scaling law

The general empirical scaling law of the exciton binding energies based on a classical model for low dimensional systems can be described as:

$$E_b = \frac{E_0}{L_W} \left(1 - \frac{\gamma e^{-\frac{2a_0}{L_W}}}{2} \right)^2$$

where E_0 and a_0 are the 3D Rydberg energy and Bohr radius of 3D perovskite, respectively, and L_W is the physical width of the quantum well.



Scheme S1. The spin-coating process of perovskite film preparation and the perovskite structure of 2D ($\text{PBA}_2(\text{MAPbBr}_3)_{n-1}\text{PbBr}_4$) films for $n = 2$ (#1), $n = 3$ (#2), $n = 7$ (#3) and 3D (MAPbBr_3) for thick (#4) and thin (#5) films.

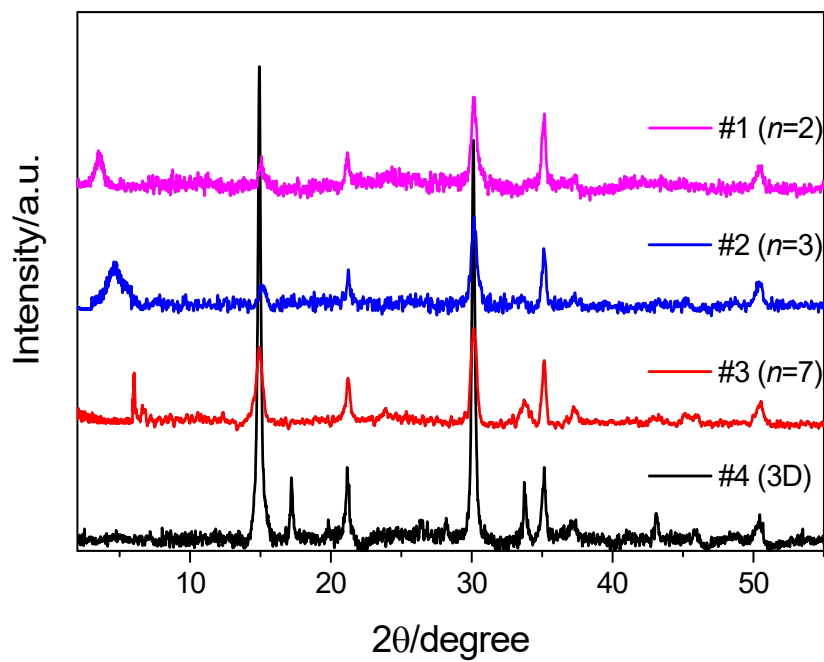


Fig. S1. The XRD patterns of #1, #2, #3 and #4.

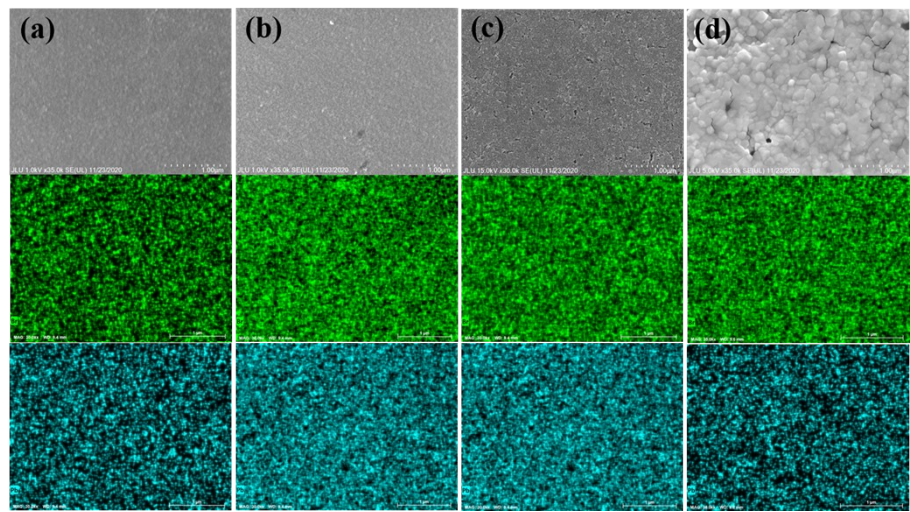


Fig. S2. SEM images and element mapping (Pb for blue and Br for green) of #1 (a), #2 (b), #3 (c) and #4 (d).

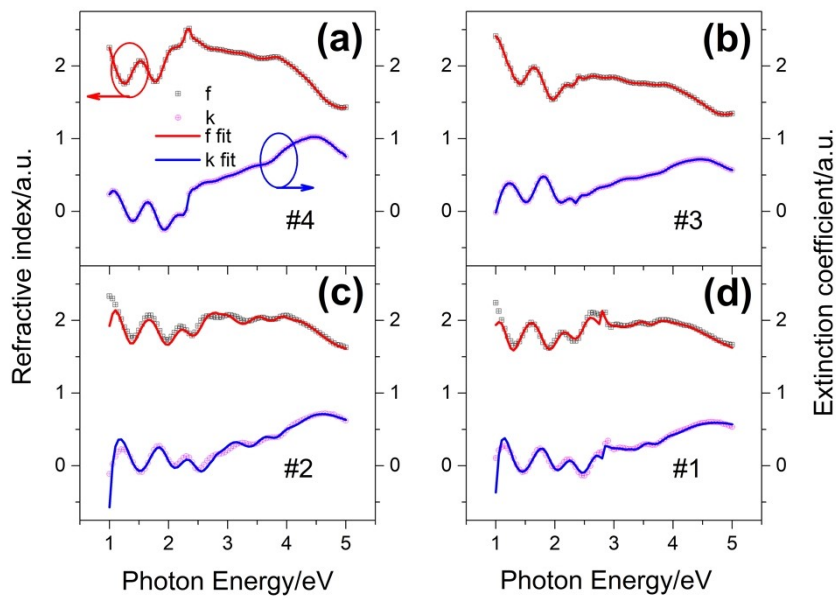


Fig. S3. Ellipsometric experimental spectra and simulated refractive and extinction coefficients dispersion relationship of #4, #3, #2 and #1. The *f* represents refractive index, and the *k* represents extinction coefficient.

Table S1. The parameters of perovskite films by fitting ellipsometric spectra, where the f_{PL} and k_{PL} are refractive index and extinction coefficient at PL peak position of perovskite films, respectively.

Perovskite	f_{PL} (a.u.)	k_{PL} (a.u.)	Thickness (nm)	Surface Roughness (nm)
#1	2.11	0.01	232.09	17.45
#2	1.83	0.03	198.21	15.23
#3	1.77	0.11	183.77	19.46
#4	2.54	0.24	201.32	18.21

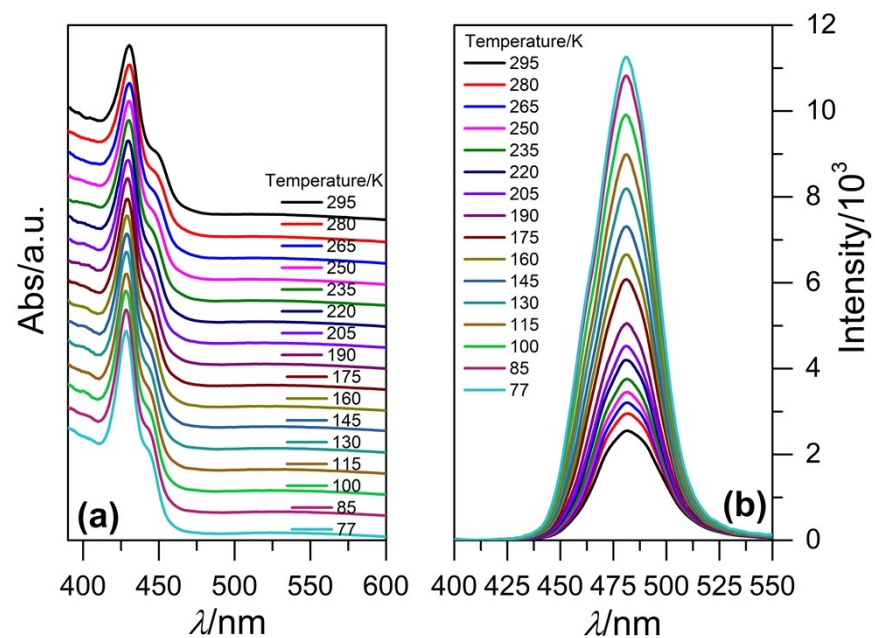


Fig. S4. Temperature-dependent absorption (a) and PL (b) spectra of #1.

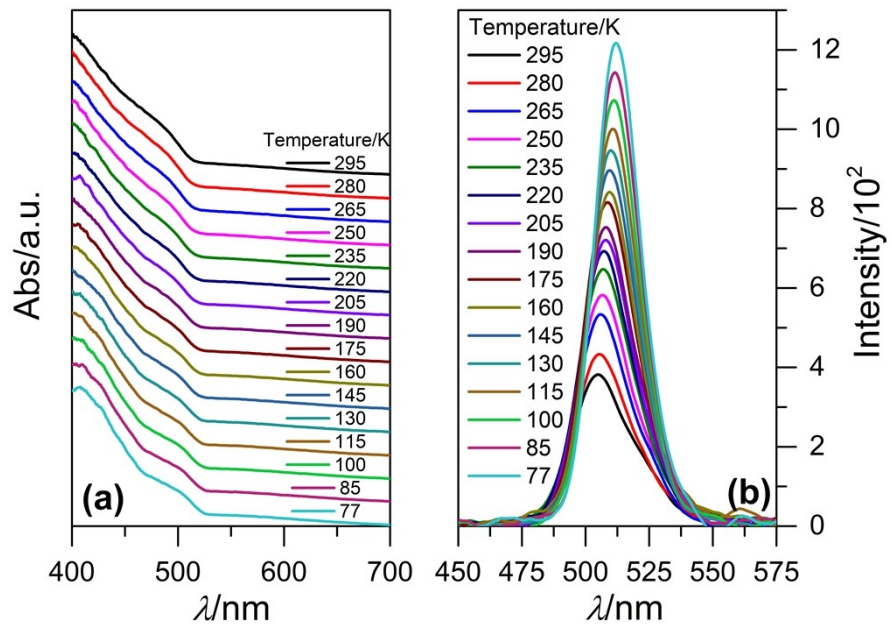


Fig. S5. Temperature-dependent absorption (a) and PL (b) spectra of #2.

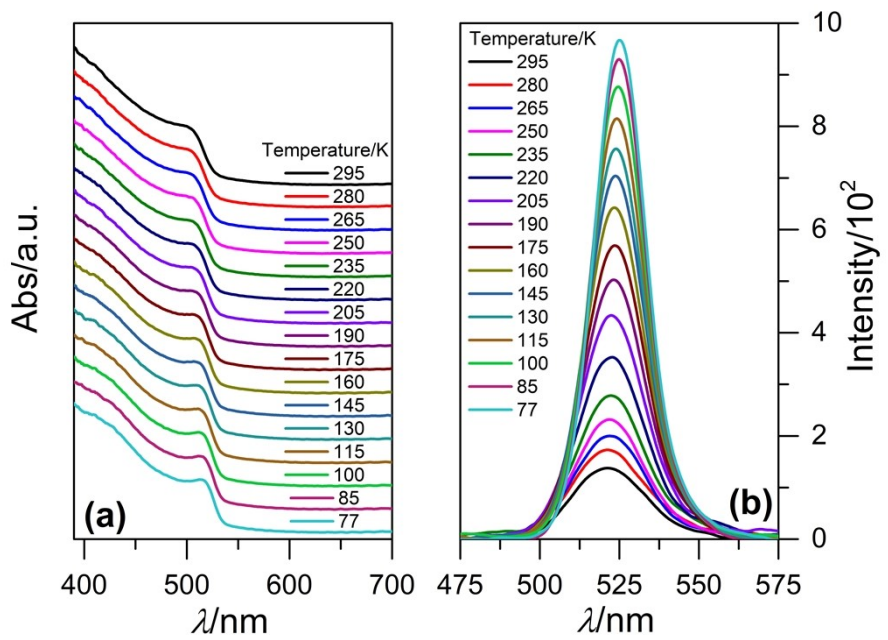


Fig. S6. Temperature-dependent absorption (a) and PL (b) spectra of #3.

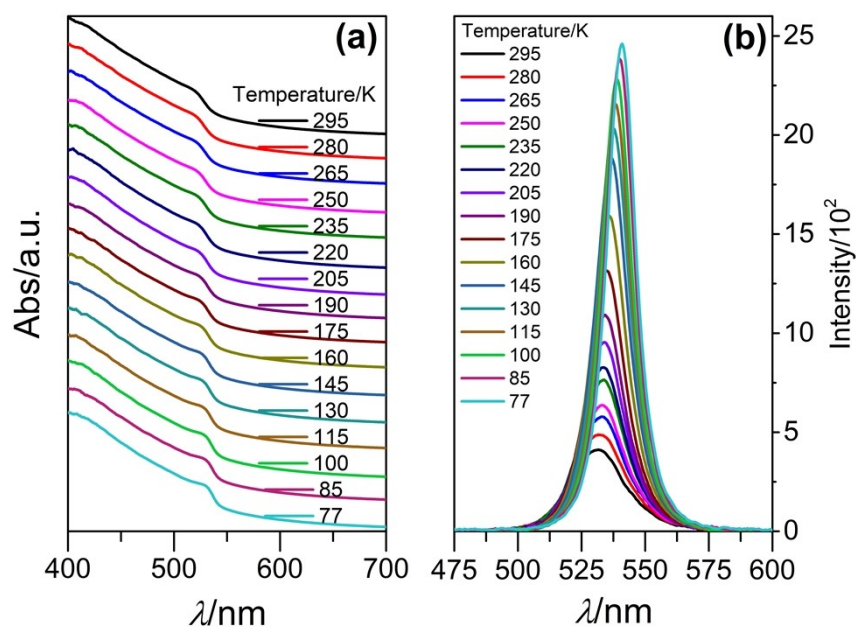


Fig. S7. Temperature-dependent absorption (a) and PL (b) spectra of #4.

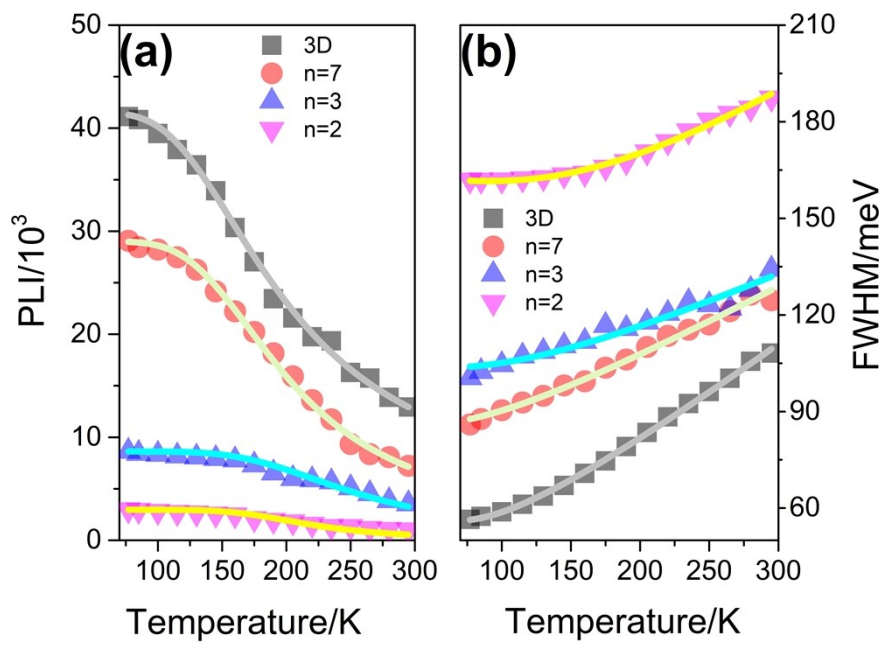


Fig. S8. Integrated PL intensity (a) and FWHM (b) as a function of temperature #4 (3D), #3 ($n = 7$), #2 ($n = 3$) and #1 ($n = 2$).

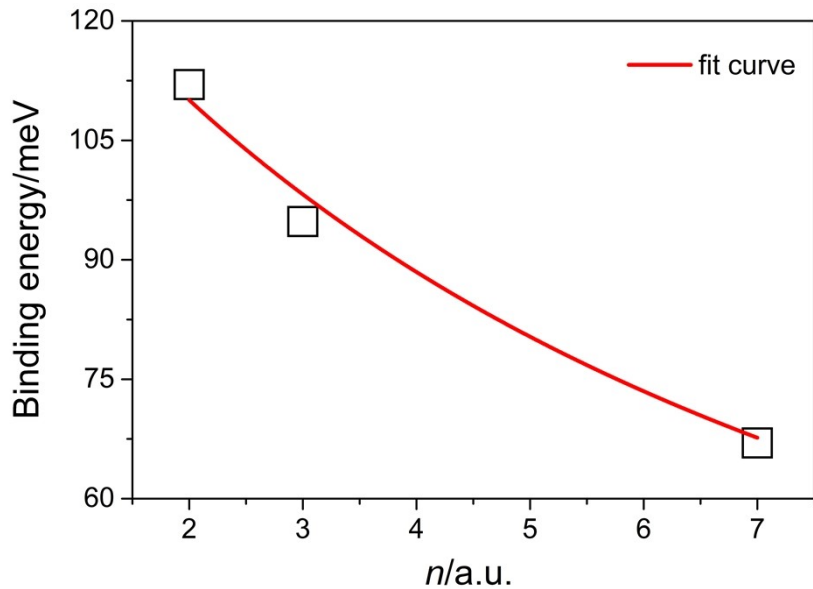


Fig. S9. The dependence between binding energy and film layer number.

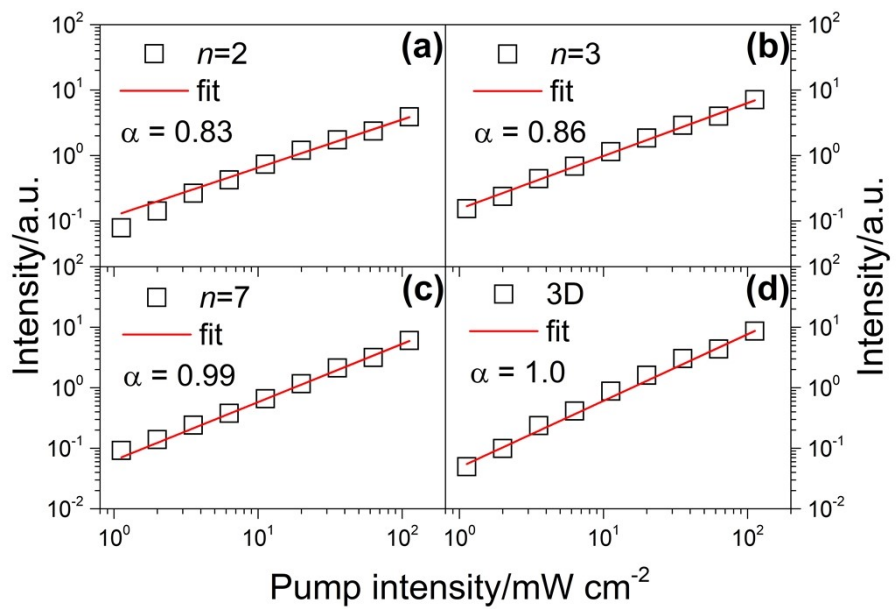


Fig. S10. The dependence between PL intensity and pump intensity which is fitted by the $I_{PL} = CP_{EL}^\alpha$.

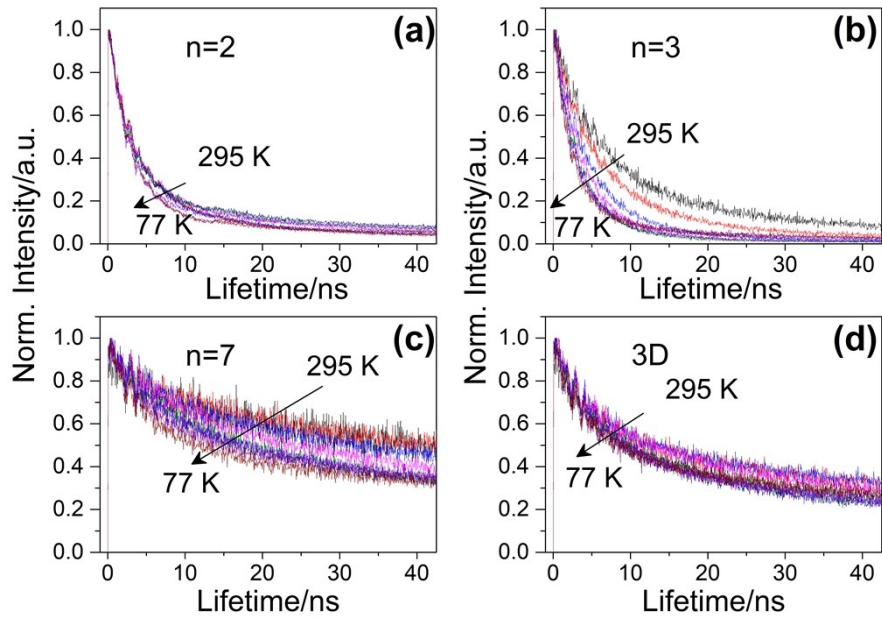


Fig. S11. Normalized PL decays of perovskite films with different layers at different temperatures.

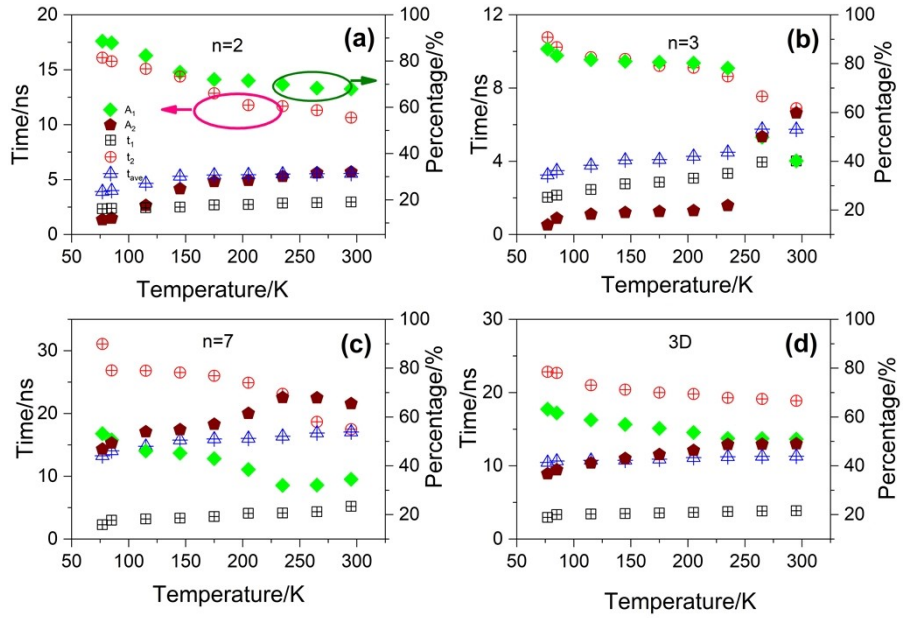


Fig. S12. The bi-exponential fitting parameters for normalized PL decay curves, where t_1 and t_2 are time parameters; A_1 and A_2 are the percentages of time parameters; t_{ave} is average lifetime.

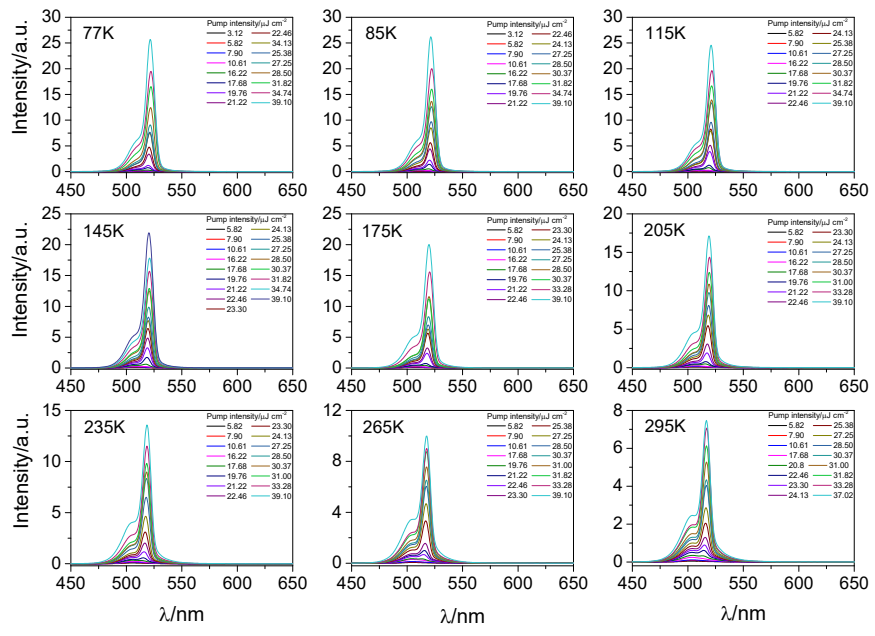


Fig. S13. Power-dependent emission spectra from #2 at different temperatures.

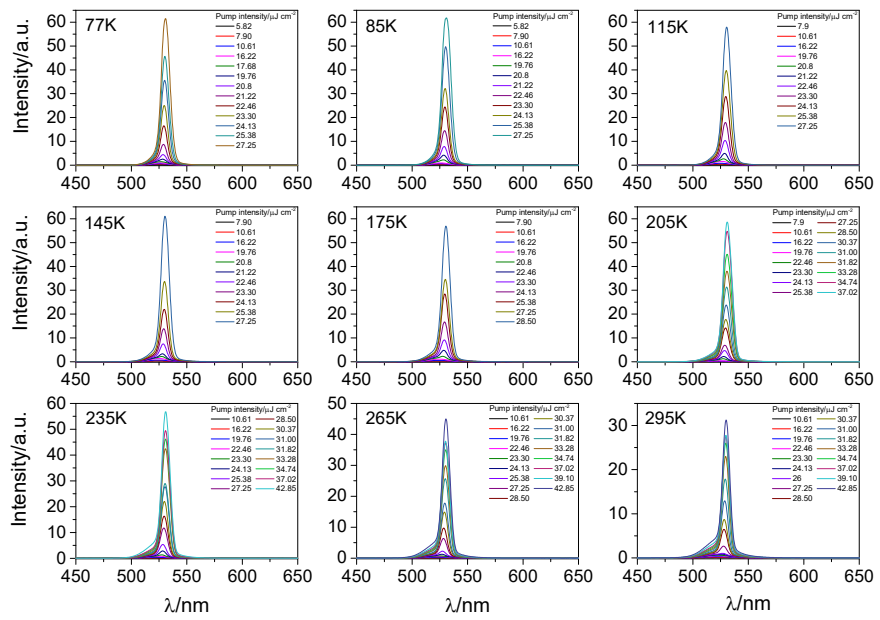


Fig. S14. Power-dependent emission spectra from #3 at different temperatures.

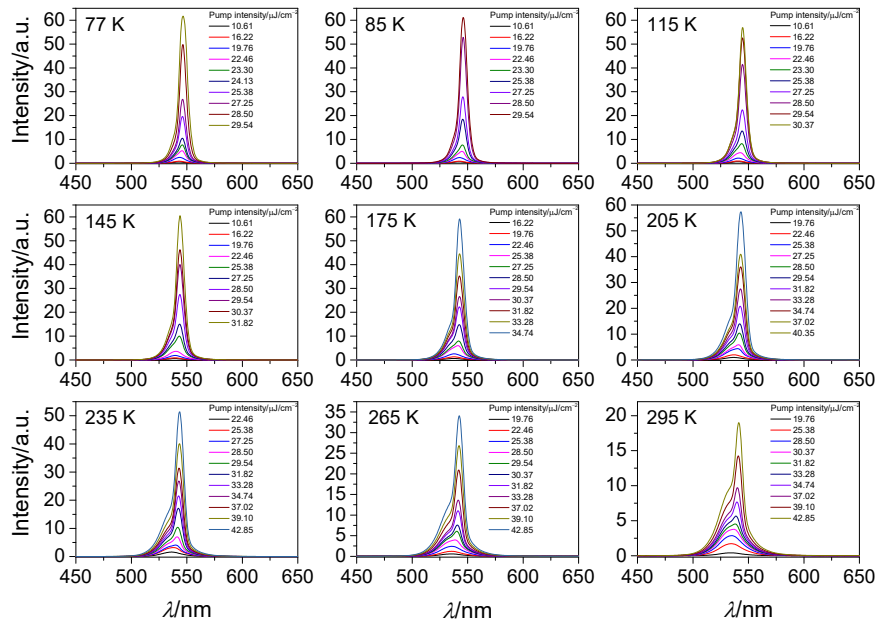


Fig. S15. Power-dependent emission spectra from #4 film at different temperatures.

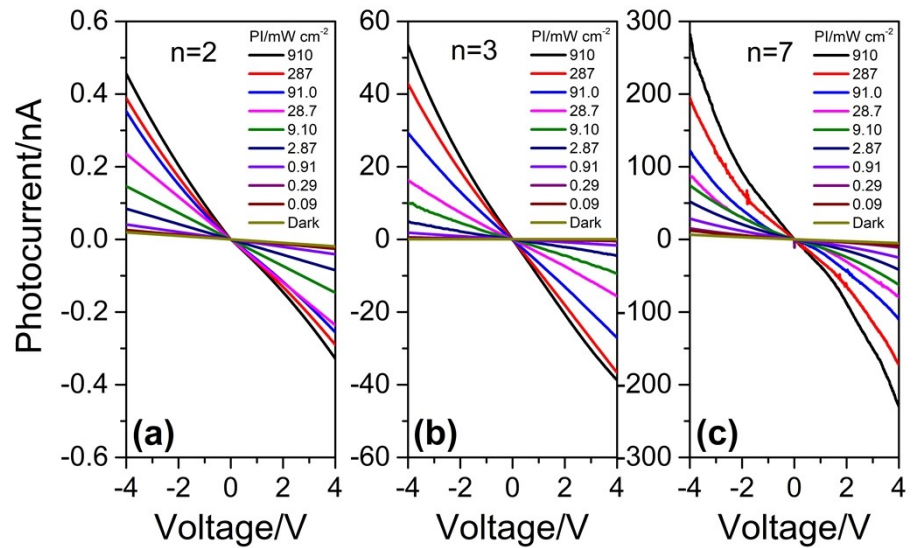


Fig. S16. I–V curves of photodetectors based on quasi-2D perovskites of #1 (a), #2 (b) and #3 (c), under different illumination intensities.